Journal of Building Engineering 43 (2021) 102548

Contents lists available at ScienceDirect

Journal of Building Engineering

journal homepage: http://www.elsevier.com/locate/jobe

Fiber-reinforcement and its effects on the mechanical properties of high-workability concretes manufactured with slag as aggregate and binder

Vanesa Ortega-López [a], Aratz García-Llona [b], Víctor Revilla-Cuesta [a, *], Amaia Santamaría [c], José T. San-José [c]

[a] Department of Civil Engineering, University of Burgos, Escuela Politécnica Superior, Calle Villadiego s/n, 09001, Burgos, Spain
[b] Fundación Centro Tecnológico de Componentes, Parque Científico y Tecnológico de Cantabria, Calle Isabel Torres, 1, 39011, Santander, Spain
[c] Department of Mechanical Engineering, University of the Basque Country, UPV/EHU, Escuela de Ingeniería de Bilbao, I (bloque B) - UPV/EHU, Plaza Ingeniero Torres Quevedo, 1, 48013, Bilbao, Spain

ARTICLE INFO

Keywords:
Slag Aggregate and binder
Fiber-reinforced high-workability concrete
Fracture toughness
Dog-bone test
Stress-strain behavior

ABSTRACT

The feasibility of manufacturing fiber-reinforced concretes of high workability through additions of high volumes of electric arc furnace steel slag is evaluated in this paper, using sustainable binders with ground granulated blast furnace slag and ladle furnace slag as a supplementary cementitious material. An extensive experimental plan is developed to test four (self-compacting and pumpable) concrete mixtures, some reinforced with 0.5% vol. of (metallic or synthetic) fibers, in both the fresh and the hardened state. Very specific mechanical aspects are examined, such as the evaluation of both longitudinal and transversal stress-strain compressive behavior, and the assessment of direct tensile strength through the "dog-bone" test. The results of testing this sustainable concrete design yielded suitable mechanical strengths, and good toughness, ductility and impact strength, among other properties. Good adhesion between the fibers and the cementitious matrix was also evident from the fiber pull-out test results. Finally, the overall results confirmed that the use of electric arc furnace steel slag can make a real contribution to construction-sector sustainability and that the mechanical behavior of these novel concretes meets the basic design requirements for use in real structures.

1. Introduction

The study presented in this paper addresses the massive reuse of industrial by-products. In particular, the conversion of waste from the steelmaking industry into value-added inputs for the construction sector. These efforts contribute both to the circular economy and to higher levels of sustainability, preserving natural resources, reducing CO_2 emissions, and decreasing the embedded energy of production processes [1]. Concrete is by far the most widely used material in the building sector, due to its versatility, durability and setting times, as well as its variable composition, which are the main reasons for such high levels of production and consumption [2]. Nevertheless, novel materials that contribute to the circular economy in concrete manufacturing processes must be treated with caution. They must never be used without previous experimental verification of the concrete in both the fresh and the hardened state. The long-term performance of a novel concrete and its durability against aggressive environmental agents must likewise be monitored [2,3].

Over the past few years, the cement industry, one of the most polluting in the world [1,4], has explored new approaches for more sustainable construction materials. These approaches cover both the reduction of the binder content and the clinker demand, replacing Portland cement with Supplementary Cementitious Materials (SCM) [1,2]. In an initial approach of this study towards the improvement of concrete sustainability, cement types II/B-S and III, as *per* EN 197-1, are used [5]. These cement types contain different proportions (from 30 to 70%) of Ground Granulated Blast Furnace Slag (GGBFS) in substitution of Portland clinker, by-product that so far has been almost exclusively used in marine environments [6] and for soil stabilization [7]. Small proportions of Ladle Furnace basic Slag (LFS) added to the concrete as an SCM are also analyzed. LFS is a by-product from the steelmaking sector that has been succesfully used in mortars and concrete [8–11], in soil stabilization [12,13] and in bituminous mixtures [14,15].

* Corresponding author. Department of Civil Engineering, University of Burgos, Escuela Politécnica Superior, Calle Villadiego s/n, 09001, Burgos, Spain.
E-mail addresses: vortega@ubu.es (V. Ortega-López), agl0053@alu.ubu.es (A. García-Llona), vrevilla@ubu.es (V. Revilla-Cuesta), amaia.santamaria@ehu.es (A. Santamaría), josetomas.sanjose@ehu.es (J.T. San-José).

https://doi.org/10.1016/j.jobe.2021.102548
Received 3 February 2021; Received in revised form 25 March 2021; Accepted 14 April 2021
Available online 22 April 2021

The second approach towards the improvement of concrete sustainability is to study the effects of Electric Arc Furnace Slag (EAFS) when used as a massive aggregate in concrete mixtures. The feasability of using EAFS both in hydraulic [16] and in bituminous mixes [17–19] has previously been demonstrated. In some fields, the use of EAFS rather than natural aggregates is often advantageous [20]. For example, its high density is useful in heavyweight concretes and radiation shields [21–23], its high polishing resistance improves the behavior of the wearing courses of pavements [24,25], and both its thermal and electrical conductivity are beneficial in special cases [26].

Self-Compacting Concrete (SCC) and pumpable concretes are undergoing global expansion, due to their significant advantages, in terms of workability and laying ranges [3]. However, they present some challenges that differ from conventional concrete, in so far as their flowability in the fresh state is essential. Careful design is therefore crucial to balance performance in both the fresh and the hardened state [27]. The right balance of alternative aggregates is a complex matter [28], as each has specific characteristics that require individual study [3]. For example, SCC containing EAFS, a high-density aggregate, has certain disavantages that involve a risk of segregation and decantation of the coarse aggregate particles suspended in the cementitious matrix, as previous studies have shown [29,30].

Metallic and synthetic fibers are also gaining larger market shares, as they can improve concrete mechanical strength and durability [31], reducing crack formation and development, and providing post-cracking loading capacity [32]. Their effects on tensile and flexural strength [33,34], fatigue resistance [35], and especially toughness [36] are clear in ordinary concrete mixtures. In general, fiber-reinforced concrete is particularly useful in pavements [37], bridge piles [38,39] and shotcrete coverings [40], although the fibers reduce flowability, therefore complicating mixing and compromising workability [40].

The research presented in this paper represents a new step forward in the workline of this research group, following a series of studies on the use of EAFS as coarse aggregate in high-workability (self-compacting) concretes and the use of SCM among other binders in those mixes. The main novelty of this paper and its contribution to research in this field is the analysis of the different fiber reinforcements and their effects within sustainable EAFS concrete mixes. The results are compared with those of a reference mixture which does not include fibers. Our aim is therefore to test whether the simultaneous use of large quantities of by-products from the steelmaking industry as both aggregate and binder is suitable for the development of high-workability fiber-reinforced concrete mixes. To do so, an extensive set of experiments is detailed for testing the mechanical behavior of these concrete mixtures. Compressive strength, tensile strength, longitudinal and tranversal stress-strain behavior, flexural strength, fracture performance, and impact and abrasion resistance are all analyzed. Furthermore, the comparison of the results with previously published articles from the literature reveals relevant conclusions on the composition of these mixtures. The analysis of all these mechanical properties contributes to a comprehensive and reliable validation of the use of these mixes in structural applications, such as bridge piles, decks, columns, beams, retaining walls and foundations.

2. Materials and methods

In this section, both the materials and the methods used in the study will be explained.

2.1. Cement, admixture, natural aggregates and water

The binders consisted of Portland clinker mixed with GGBFS, an industrial by-product recovered from blast furnaces, in order to enhance the general sustainability of concrete manufacturing. Two types of cement were used in the present article. Firstly, a Portland cement type II/B-S 42.5-N containing 30% Ground Granulated Blast Furnace Slag (GGBFS), and secondly, a Portland cement type III/B 32.5-N containing 70% GGBFS, in accordance with EN 197-1 [5]. Furthermore, a small fraction (6% of total binder) of Ladle Furnace Slag (LFS) [41–43] was also added to the pumpable mixture (IIIP) as an SCM. The binder variable was introduced to show the influence of the different cement types on both the workability and the mechanical strength of the concretes. It was also introduced to study the mechanical response of the hardened fiber-reinforced concrete in terms of the interaction between the slag aggregates and the mineral additions of GGBFS within the cement mix.

The admixture, a carboxylate-based water emulsion, previously shown to have enhanced the workability of concretes manufactured with EAFS [44], acting as plastizicer and viscosity conditioner, was provided by CHRYSO®™. The mix water, taken from the urban mains supply of the city of Burgos (Spain), contained negligible amounts of compounds that could affect the preparation of hydraulic mixtures.

The limestone fines used (Fig. 1) in the mixes consisted almost exclusively of calcite (>95%). They had a gradation fraction of 0/1.18 mm (ASTM passing sieve Nº 16), a fineness modulus of 1.5 units, a specific gravity of 2.65 Mg/m^3 and a water absorption rate of 0.53%. Their gradation curve is shown in Fig. 2. This limestone fine fraction compensated the lack of fine fraction particles in the EAFS fine aggregate (<4 mm), improving workability and preventing segregation [45].

2.2. EAF and LF slag physic-chemical properties

Electric Arc Furnace Slag (EAFS) was supplied from the company Hormor-Zestoa in the form of a high-density angular-shape aggregate (around 3.4 Mg/m^3) with two grading sizes (fine <4 mm, medium 4/12 mm), as shown in Fig. 1. It was used after crushing and three months of spontaneous weathering. The chemical composition, the results of X-ray diffraction (XRD) analysis, and some of its physical properties are shown in Table 1. Its fine and medium fractions, shown in Fig. 2, had fineness moduli of 3.9 units and 5.7 units, respectively. Details on this material can be found in several publications by this research group [44,46].

A high-silica low-alumina Ladle Furnace Slag (LFS) with a powdery appearance, grain sizes of under 1 mm, and a fineness modulus of 0.75 units was used. Its chemical composition and XRD analysis results are also shown in Table 1. Some LFS compounds showed binding properties

Fig. 1. Used aggregates: EAFS 4/12 mm (left); EAFS 0/4 mm (middle); limestone fines 0/1.18 mm (right).

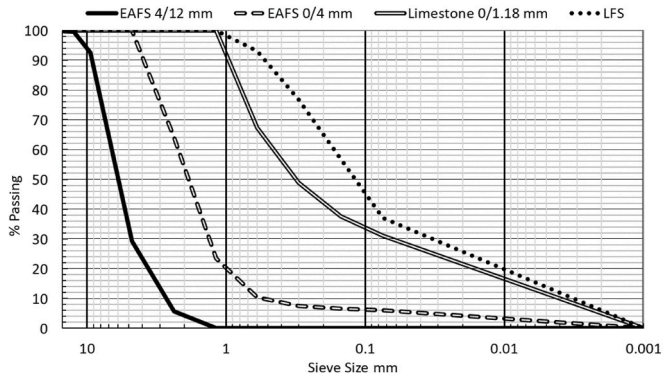

Fig. 2. Grading of aggregates and LFS.

Table 1
EAFS and LFS chemical compositions and physical characteristics.

Compounds	EAFS	LFS
Fe_2O_3 (%)	22.3	1.1
CaO (%)	32.9	59.2
SiO_2 (%)	20.3	21.3
Al_2O_3 (%)	12.2	8.3
MgO (%)	3.0	7.9
MnO (%)	5.0	0.3
SO_3 (%)	0.4	1.4
Cr_2O_3 (%)	2.0	–
P_2O_5 (%)	0.5	–
TiO_2 (%)	0.8	0.2
Others (Na_2O, K_2O …)	0.6	0.4
Angularity coefficient BS-812	close to 11 units	
Water absorption (%)	1.12	–
Specific gravity (Mg/m^3)	3.42	3.03
XRD analysis results	Wüstite-Ghelenite-Kirsteinite	Periclase-Olivine-mayenite

similar to an SCM, as noted in several studies [41–43,47]. The remainder of the LFS can be considered as a slightly expansive fine aggregate fraction; its expansiveness presents no risk, due to its low proportion in the global mix.

2.3. Fibers

Metallic and synthetic fibers, with the characteristics shown in Table 2, were separately used in the mixtures. Steel fibers, labelled M (hooked-end wire pieces), and polypropylene fibers, labelled Y (surface-dimpled) were added to optimize the efficacy of the mix through their adherence with the surrounding cementitious matrix.

Table 2
Fiber characteristics.

Characteristic	Metallic fibers (M) (Arcelor Mittal HE 55/35)	Synthetic fibers (Y) (SikaFiber T-35)
Material	Steel	Polyolefin/polypropylene
Length (mm)	35	35
Equivalent diameter (mm)	0.55	0.93
Length/diameter aspect ratio	64	38
Tensile strength (MPa)	>1200	>400
Density (kg/m^3)	7900	910
Young's modulus (GPa)	210	6

2.4. Mix design

In this study, four different concrete mixtures were studied using two types of cement (CEM II/B-S 42.5-N and CEM III/B 32.5-N), in amounts of around 310–330 kg/m^3 to reach a compressive strength at 28 days of between 30 and 50 MPa, and a volume of (metallic and synthetic) fibers at around 0.5% of the concrete mass. Their common aspects were the ideal gradation with the Fuller-Bolomey curve with an exponent within the range of 0.45–0.5 units, a water/binder ratio of around 0.5 units and a high volume of added EAFS. The suitable proportioning of concrete mixes containing EAFS has been widely analyzed and described in previous works [44] by this research group, using the maximum volume of slag above which the behavior in the fresh state is inadequate. In conventional terms, the in-weight replacement of natural aggregate with EAFS was around 60% in the self-compacting mixes and around 70% in the pumpable mix, as shown in Table 3. It may be also recalled that highly workable mixtures are indispensable when producing efficient high-workability structural concretes, which implies limiting the fiber content to the proposed value of 0.5%.

- Mixtures IISC, IISC-M and IISC-Y were self-compacting concretes, containing CEM II/B-S 42.5-N and either metallic (IISC-M) or synthetic (IISC-Y) fibers. Mixture IISC, the reference mix of this study, incorporated no fibers to analyze the effect of their addition. The mix proportions were defined to achieve a slump flow of around 600 mm, and a t_{500} (time to reach a slump flow higher than 500 mm) lower than 5 s in the fiber-containing mixtures.
- Mixture III-P was a pumpable concrete in which the binder included two components: CEM III/B 32.5-N and LFS (6% of the total amount of binder) as SCM [42,43]. In addition, metallic fibers were also added. In this case, the workability target was a slump higher than 160 mm (S4 consistency) in the Abrams cone test.

Table 3 depicts the mix design of each mixture and Fig. 3 (calculated in volume) shows the mix gradation, together with the Fuller's curve. Two aspects must be highlighted regarding this mix design: the volumetric calculations and the effect of the admixture.

- Regarding the volume of each component, the same amount of binder was added to all mixtures (10.5% of total volume). However, the self-compacting mixes need additional fine fractions to achieve the desired workability, which explains their higher limestone fines content (EAFS and limestone fines in proportion to the volume of the mix were 40 and 35%, respectively, for self-compacting mixes, and 50 and 25% for pumpable concrete).
- As previous studies from this research group have shown [44], the amount of admixture could not exceed 2% of the binder mass in any

Table 3
Mix proportions in kg per cubic meter of concrete.

Components in kg	IISC	IISC-M	IISC-Y	IIIP-M
Cement II/B-S 42.5R	325	325	325	–
Cement III/B 32.5 N	–	–	–	315
LFS	–	–	–	25
Water	170	180	185	160
EAFS medium (4/12 mm)	755	755	755	935
EAFS fine (0/4 mm)	545	545	545	685
Limestone fines (<1.18 mm)	955	955	955	655
Admixture	5.0	5.0	5.0	4.2
Fiber reinforcement: type/kg (0.5% vol.)	–	M/40	Y/4.5	M/38
Total weight	2755	2765 (*)	2770 (*)	2780

Roman number II and III: type of Portland cement according EN-197-1 [5].
P = pumpable; SC = self-compacting. M = metallic fiber; Y = synthetic fiber.
(*) = the proportioning of these mixtures amounts 1030 L.

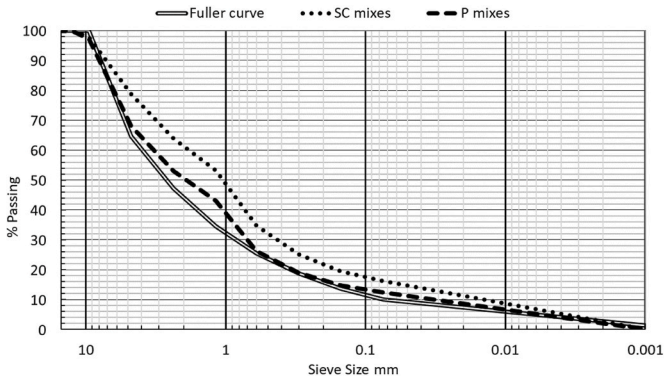

Fig. 3. Approximate gradation of the mixtures.

mix, due to the appearance of segregation in the slump-flow and the Abrams cone tests. For this reason, self-compactability was achieved by increasing the amount of water and limestone fines. In mixture IIIP-M, this self-compactability could not be obtained, because of the poor interaction between the admixture and the large amounts of GGBFS that were incorporated in CEM III/B, so the target consistency was defined as S4.

2.5. Specimen preparation and testing program

The mixing sequence involved a blend of aggregates for 1 min. Then, the cement and the water were added, followed by 2 min of mixing. Subsequently, the admixture was poured followed by 3 min of mixing. Finally, the fibers were added when the mixture was homogeneous, and the concrete was mixed for another minute. Once the mixing process had been completed, in-fresh state tests were performed, following the EFNARC recommendations [48] and the specifications of standard EN 206 [49]. Subsequently, the specimens were prepared to perform each test in the hardened state, as detailed in Table 4.

The specimens were cured in a chamber at temperature and moisture levels of 20 ± 2 °C and 95 ± 5%, respectively, over different periods, until the age of testing (detailed in Table 6). The numerical results of the test for characterizing the material represent the average of at least three specimens that showed coherent values. The standard deviation is also shown in brackets alongside these values.

The test plan included flowability tests in the fresh state and a complete mechanical characterization in the hardened state: behavior under compressive loading, including compressive strength, modulus of elasticity, Poisson coefficient, and longitudinal and transversal stress-strain curves, indirect tensile strengths (Brazilian test and flexural test), direct (uniaxial) tensile strength with the "Dog-bone" test, bending tests with and without notching, with results of toughness, fracture energy, and post-cracking behavior tests, fiber pull-out test, impact strength, and abrasion resistance. In this extensive experimental program, the validity of the developed mixtures is reliably demonstrated for use in structural applications, analyzing all possible loading scenarios to which the developed mixtures may be subjected. Furthermore, the performance of the mixes is compared with results available in the literature, which addresses the behavior of fiber-reinforced high-workability concrete manufactured with conventional binder and aggregates.

Table 4
Tests and corresponding specimens.

Test	Standard [5]	Specimens
Hardened density	EN 12390-7	Cylindrical specimens of 100 × 200 mm
Compressive strength, elastic modulus and stress-strain behavior	EN 12390-3 EN 12390-13	
Splitting tensile strength	EN 12390-6	Cylindrical specimens of 150 × 300 mm
Impact strength	UNE 83514 [50]	
Direct tensile strength [51]	–	Customized Dog-bone specimens (explained in section 4.5)
Flexural strength	EN 83509	Prismatic specimens of 100 × 100 × 400 mm
Flexural toughness, first crack strength and fracture energy	EN 83510	
Flexural toughness, Limit Of Proportionality (LOP) and residual flexural strength	EN 14651 + A1	Notched prismatic specimens of 150 × 150 × 600 mm
Abrasion resistance	EN 1340 and EN 14157	Cubic specimens 10 × 10 × 10 mm
Fiber pull-out	ASTM C900-19 [52] ACI 228.1R-19 [53]	Prismatic specimens of 75 × 75 × 285 mm

3. Fresh properties of concretes

Concrete in the fresh state can be considered self-compacting or pumpable when it meets standardized values for flowability, viscosity, segregation resistance, and passing ability. These requirements are defined in future applications and the desired performance of the concrete, influenced by the geometry of the element that is cast, the laying equipment, the formwork and the containment level, *etc*. Table 5 summarizes the fresh properties of the mixtures under study.

The spreading on a steel plate of the self-compacting mixtures was measured in accordance with EFNARC recommendations [48] and standard EN 206 [49]. Mixture IISC was classified as SF2 (660–750 mm) while the presence of fibers decreased the flowability of mixtures IISC-M and IISC-Y, which were classified as SF1 (550–650 mm). In the L-box test, only performed on the self-compacting mixture without fibers, IISC, the PA2 class (≥0.80, with 3 rebars) that it achieved was considered suitable for self-compactability. The pumpable mixture IIIP-M achieved a S4 consistency class (slump between 160 and 210 mm) in the Abrams cone test. This mixture showed acceptable flowability for pumping, requiring slight vibration for proper placement, as was expected. The loss of flowability when adding metallic fibers to the mixes under study, with a high EAFS content and the consequent slight increase in the added water, of over 10%, was higher than the increase observed in concrete made with natural aggregate, where the addition of the same fiber content led to a loss of flowability of around 5% [54,55]. It is possible that the high density of the slag was combined with the negative effect of the fibers, thus amplifying the flowability decrease, an aspect previously described in relation to vibrated concrete by the same research group [36].

The fresh density values were in the range of 2.60–2.70 Mg/m^3 for all the mixtures. They were heavier than a conventional concrete, the fresh density of which was around 2.5 Mg/m^3, due to the greater specific gravity of the EAFS aggregate [16]. When the fibers, especially the

Table 5
Fresh properties of the mixtures.

Property	Standard [5]	IISC	IISC-M	IISC-Y	IIIP-M
Slump/Spreading (mm)	EN 12350-8/12350-2	-/720	-/650	-/620	175/-
Consistency/flowability class	EN 206	-/SF2	-/SF1	-/SF1	S4/-
L-box (passing ability, 3 bars)	EN 12350-10	0.82 (PA2)	–	–	–
Fresh Density (Mg/m^3)	EN 12350-6	2.71	2.67	2.60	2.71
Occluded air (%)	EN 12350-7	2.2	2.0	1.9	3.6

synthetic ones, were incorporated in the mix, the value of this density decreased due to the increasing addition of water.

The amount of vacuolar/spherical porosity, evaluated with the occluded-air test, was considered at reasonable levels in almost all mixtures (about 2%). However, the air content was higher in mixture IIIP-M (3.6%), with a higher content of GGBFS and LFS. This fact is attributed to physical-chemical (adsorption-radical, hydrophilic-hydrophobic) interactions between the finest particles of the binder and the admixture [41], which normally favors the formation of air bubble micro-pores [56].

4. Hardened properties of concretes

This section contains the results of the hardened properties of the four concrete mixtures under study, summarized and shown in Table 6. Each test and their results are explained in the following sub-sections.

4.1. Density, compressive strength and elastic properties

In this section, the density and the conventional mechanical properties of concrete (compressive strength, modulus of elasticity, and Poisson coefficient) are analyzed.

4.1.1. Density and compressive strength

As can be seen in Table 6, the hardened densities of the concretes varied from 2.54 to 2.65 Mg/m^3. The volumetric fraction of EAFS and the porosities (capillary, vacuolar) of the mixture matrices were the key variables to justify these results. The compressive strength results measured at 7, 28, 90, 180 and 360 days of curing (fc_7, fc_{28}, fc_{90}, fc_{180} and fc_{360}, respectively) are also detailed in Table 6.

The evolution of concrete compressive strength showed that at early ages (until 28 days) the mixtures could be divided into two classes according to the type of cement. Mixture IIIP manufactured with CEM III/B (70% GGBFS) and LFS, reached around 30 MPa at 28 days, while the mixtures manufactured with CEM II (30% GGBFS) reached around 50 MPa at the same age. Hence, both types of cements could be considered suitable to produce sufficiently strong structural concrete and any strength loss was noticeable with increased amounts of GGBFS. The evolution of this property with age was similar when measured as the ratio between fc_7 and fc_{28} and between fc_{90} and fc_{360}: 72–78% and 87–98%, respectively, in all cases. Analyzing the effects of the different cements, the compressive strength of the IIIP-M mix was roughly half of IISC mixture at all ages. The excellent long-term strengths of the self-compacting concretes, especially visible in mixture IISC, were due to the very good quality of the matrix, with suitable gradation and limestone fines balance [57]. There was no increase in the compressive strength of SCC following the addition of fibers, unlike usual when adding fibers to natural aggregate concrete [56,58]. The increased amount of water required for high workability, led to an increase in the water/binder ratio.

The addition of by-products and the particular dosage required to achieve a high workability can alter the development of strength over time compared to conventional concretes. For this reason, the validity of three of the most widely accepted models in the literature for the evolution of compressive strength in conventional concretes over time is analyzed. These models reflect isothermal curing such as the one carried out in this study and are shown in Table 7. It can be seen that they permit the compressive strength (*CS*, in MPa) to be obtained as a function of the age of curing (*t*, in days). The remaining elements are adjustment parameters, the values for which can be obtained with a multiple regression.

As can be seen in Table 8, these models were properly fitted, with coefficients R^2 above 90% in all cases, which reflects their suitability for mixtures made with EAFS, sustainable binders and fibers. The concretes with fibers achieved a coefficient R^2 of 99% in at least one model, the exponential model presenting the best fit. The fit for mixture IISC was slightly worse (maximum coefficient R^2 of 97%), while the modi-

Table 6
Hardened properties of concretes. Standard deviation in brackets.

Property		IISC	IISC-M	IISC-Y	IIIP-M
Hardened density (Mg/m^3)	90 days	2.63 (0.3)	2.57 (0.3)	2.54 (0.2)	2.65 (0.3)
Compressive strength (MPa)	7 days	47.1 (1.5)	38.2 (0.4)	33.3 (0.1)	20.2 (0.3)
	28 days	59.7 (5.7)	53.1 (1.5)	46.1 (1.0)	27.4 (1.3)
	90 days	75.3 (4.1)	63.6 (3.6)	56.8 (5.3)	33.3 (1.0)
	180 days	76.1 (3.5)	65.2 (3.5)	59.1 (3.2)	38.1 (2.1)
	360 days	77.9 (0.2)	68.8 (5.3)	60.5 (2.7)	42.2 (1.2)
Modulus of elasticity: E (GPa)	90 days	40.1 (0.7)	34.7 (1.5)	31.6 (0.9)	26.1 (0.5)
Poisson coefficient (ν)	90 days	0.23 (0.1)	0.22 (0.1)	0.22 (0.1)	0.19 (0.1)
Flexural strength (MPa)	90 days	7.93 (2.3)	5.97 (1.1)	5.04 (0.3)	4.43 (0.5)
Splitting tensile strength (MPa)	90 days	5.11 (0.4)	4.84 (0.6)	4.35 (0.4)	3.36 (0.4)
Direct tensile strength (MPa)	160 days	4.25 (0.2)	3.77 (0.4)	3.66 (0.4)	3.14 (0.2)
(Tensile) Young's modulus (GPa)	160 days	38.5 (1.0)	37.9 (2.8)	35.5 (0.3)	32.3 (0.1)
Pull-out test (at 180 days)	Ultimate load (N)	–	310 (119)	191.4 (27)	250.1 (30)
	Pull out length (mm)	–	1.5 (0.3)	1.9 (0.5)	1.3 (0.1)

Table 7
Models of compressive strength development over time.

Model	Expression	Parameters
Carino and Lew [59]: hyperbolic model	$CS = S_u \cdot \frac{k\cdot(t-t_0)}{1+k\cdot(t-t_0)}$	S_u: limiting strength (MPa) k: constant of strength development (day^{-1}) t_0: age at start of strength development (days)
Kundsen [60]: modified hyperbolic model	$CS = S_u \cdot \frac{\sqrt{k\cdot(t-t_0)}}{1+\sqrt{k\cdot(t-t_0)}}$	
Hansen and Pedersen [61]: exponential model	$CS = S_u \cdot exp\left(-\left(\frac{\tau}{t}\right)^{\alpha}\right)$	S_u: limiting strength (MPa) τ: time constant (days) α: shape parameter in the linear portion

Table 8
Fitted parameters of compressive strength development over time.

Model	Parameter	IISC	IISC-M	IISC-Y	IIIP-M
Carino and Lew [59]: hyperbolic model	S_u (MPa)	77.79	68.27	60.63	42.35
	k (day^{-1})	0.19	0.18	0.16	0.06
	t_0 (days)	0.00	0.00	0.00	0.00
	Coefficient R^2 (%)	93.64	99.32	97.27	91.85
Kundsen [60]: modified hyperbolic model	S_u (MPa)	89.20	76.79	69.24	50.66
	k (day^{-1})	0.19	0.21	0.18	0.05
	t_0 (days)	0.53	2.36	2.21	0.00
	Coefficient R^2 (%)	**97.13**	99.56	99.10	98.58
Hansen and Pedersen [61]: exponential model	S_u (MPa)	88.84	72.68	67.67	97.61
	τ (days)	2.63	3.32	3.62	125.96
	α	0.44	0.59	0.50	0.16
	Coefficient R^2 (%)	97.09	**99.75**	**99.23**	**99.79**

fied hyperbolic model showed the best fit. The best-fit model for each mixture is shown in Fig. 4.

4.1.2. Elastic properties

The elastic properties (Table 6), modulus of elasticity and Poisson's coefficients of the CEM II mixtures, after 90 days in the moist room, showed a modulus of elasticity between 30 and 40 GPa, while the CEM III/B mixture only reached 26 GPa. However, the Poisson's coefficients were 0.22 units in almost all cases, slightly lower in mixture IIIP-M (0.19 units), consistent with the compressive strength results, and assuring good homogeneity.

The modulus of elasticity is usually estimated using linear or exponential equations depending on compressive strength (f_c) [62]. For normal strength concrete, the standards of the American Concrete Institute (ACI-318) [63] and the International Federation for Structural Concrete (CEB-FIB) [64] express this relationship through equations (1) and (2), respectively.

$$E = 4,700 \cdot \sqrt{f_c} \tag{1}$$

$$E = 21.5 \cdot 10^3 \cdot \left(\frac{f_c}{10}\right)^{\frac{1}{3}} \tag{2}$$

In Fig. 5, the theoretical curves, calculated with equations (1) and (2) are compared with the experimental results at 90 days. The adjustment to ACI-318 is more precise, but for all the mixtures the experimental values were below the theoretical values, *i.e.*, the results of applying both structural codes slightly overestimated the moduli of elasticity of these EAFS concretes. It can also be observed that the presence of the fibers worsened the fitting of the curve.

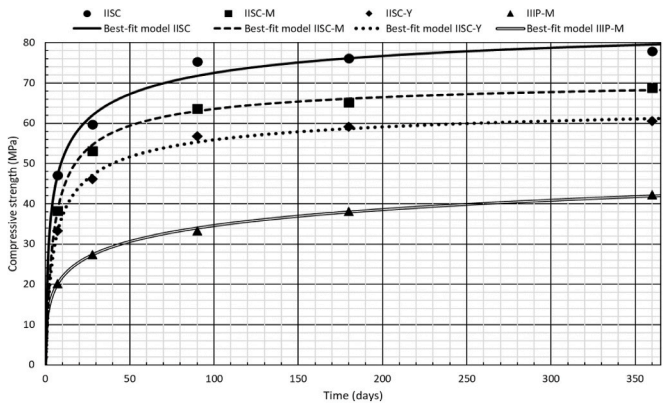

Fig. 4. Compressive strength development over time.

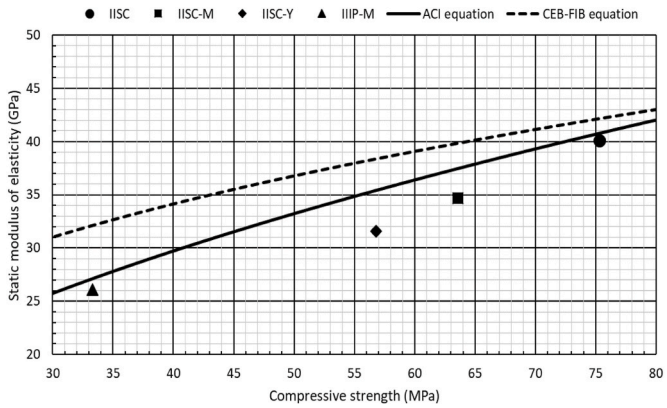

Fig. 5. Relationship between elastic modulus and compressive strength at 90 days.

Finally, as a global reflection, a relevant aspect must be highlighted. Starting with the "reference mixture" IISC, which showed the highest strength and stiffness, it was observed that the addition of fibers to that initial mixture (mixtures IISC-M and IISC-Y) led to heightened water demand, in order to maintain a suitable self-compacting workability and, as a result, the compressive strength and the stiffness decreased in these two fiber-containing mixtures, despite any presumable increase in strength and stiffness produced by the presence of reinforcement fibers [65,66]. This phenomenon has also been observed in SCC with natural aggregate [58].

4.2. Stress-strain behavior under compression load

Three cylindrical specimens 100 mm in diameter, cured for one year in moist room, were subjected to compressive loading up until failure, in order to define the stress-strain behavior in the plastic region developed by the mixtures. In this way, both longitudinal and transversal strain was measured and recorded using strain gauges and a data logger. The stress-strain curves are shown (in black) in Fig. 6.

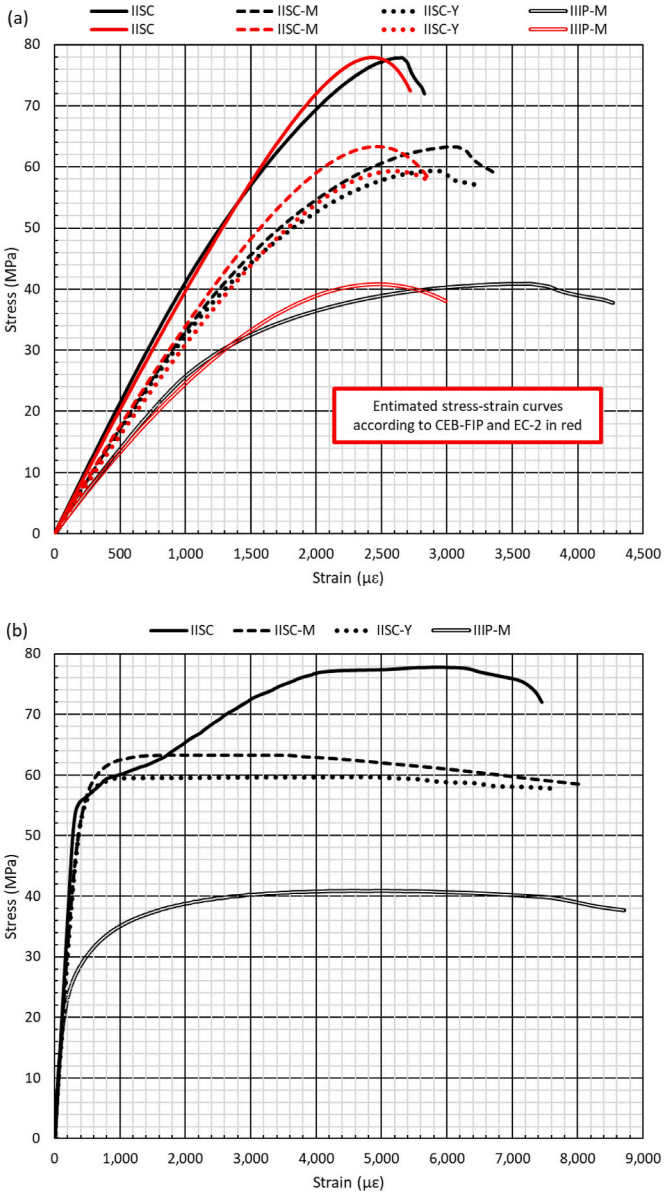

Fig. 6. Stress-strain curves of the compression test: (a) longitudinal direction; (b) transversal direction.

Regarding the longitudinal direction, mixture IISC had the most rigid elastic behavior (highest modulus of elasticity). In the plastic region, strain at failure was the lowest for the aforementioned mixture (2654 με), not even reaching the theoretical failure strain advanced in structural standards (3500 με) [63,67,68]. Mixtures IISC-M and IISC-Y showed an intermediate behavior of greater similarity to conventional concretes, with a fracture strain of around 3300 με. The increased strain when adding metallic fibers was 15%, similar to the one observed in SCC made with natural aggregate [54]. The use of synthetic fibers did not modify the behavior observed in the conventional SCC [69]. Mixture IIIP-M presented the highest deformability up until failure (4269 με). The other aspect to highlight is the fact that the higher the failure strain, the lower the deformation of the Limit Of Proportionality (LOP) (for example, 1131 με for mixture IISC and 876 με for mixture IIIP-M). In brief, the greater stiffness of the mixtures resulted in elastic behavior with greater deformations, although the mixtures had a lower failure strain limit.

The Model Code of CEB-FIP [64], and Eurocode 2 (EC-2) [67] provide formulations for estimating the stress-strain curve of concrete (equations (3)–(5)), which depend on the compressive strength of the concrete (R) in MPa and its modulus of elasticity (E) in GPa. σ (MPa) and ε (με) represent the stress and the strain of the different points of the stress-strain curve, respectively.

$$\sigma = \frac{R \cdot \left[K \cdot \left(\frac{\varepsilon}{\varepsilon_0}\right) - \left(\frac{\varepsilon}{\varepsilon_0}\right)^2\right]}{1 + (K-2) \cdot \left(\frac{\varepsilon}{\varepsilon_0}\right)} \tag{3}$$

$$K = 1 + 2 \cdot e^{-\left(\frac{R}{40}\right)} \tag{4}$$

$$\varepsilon_0 = \left[4 + 3 \cdot K + \sqrt{(4 + 3 \cdot K)^2 - 40}\right] \cdot \frac{100 \cdot R}{E} \tag{5}$$

Fig. 6a shows that the estimation of the stress-strain curve for the IISC mix was acceptable. The stress-strain behaviors of both the EAFS and the natural aggregate concretes were not so dissimilar. The addition of fibers, both metallic and synthetic, clearly caused this model to underestimate the strain at maximum load. However, while EAFS aggregate did not excessively affect this behavior, the use of slag as binder had a very noticeable effect, since the IIIP-M mix (GGBFS content of 70% of the total amount of binder) showed a much higher deformability in the plastic zone than expected according to this model.

In the transversal direction, the linear elastic region was adjusted by the Poisson's coefficient, and the aspects of plastic deformability discussed above regarding the longitudinal direction were also valid, although the plastic strain at failure point was much higher, due to the bulging of the cylindrical specimens. The fracture strain of the mixtures was reached within the interval between 7410 and 8706 με. However, three different types of behavior could be distinguished. On the one hand, mixture IISC, the only one without fibers, had a yielding step at the end of the elastic zone (75% of the maximum stress). Mixtures IISC-M and IISC-Y were characterized by their high strain with practically no increase in stress within the yielding (almost horizontal) region where the maximum of the curve is almost imperceptible. Finally, the stress-strain curve of mixture IIIP-M showed a very similar curved shape to the one in the longitudinal direction. Although CEM III/B also had fibers, as the load was applied, it caused a more progressive increase in transversal deformation than in the mixtures containing CEM II/B-S. If the transversal strains of the IISC-Y mix are compared with those obtained in the SCC reinforced with a similar content of synthetic fibers, it can be observed that the use of EAFS may have caused the SCC to admit higher transversal strains before failure [69].

Table 9 summarizes the most relevant values of these curves, which clearly illustrates the aspects discussed in this section. In addition, this table shows the energy that the mixtures absorbed during this test, following the calculation of the area under the curve, having applied the trapezoidal rule. The level of absorbed energy showed that mixture IISC-M was the one with the highest absorption capacity, due to its greater deformability, compared to mixture IISC, in spite of its greater strength. Mixture IIIP-M provided a higher energy absorption capacity than mixture IISC-Y, showing that the addition of synthetic fibers led to a lower energy dissipation capacity, mainly due to the decrease of compressive strength, because of the greater amount of water needed to reach self-compactability.

The relationship between the longitudinal and transversal strain throughout the loading process can be seen in Fig. 7, in which the elastic field, associated with a Poisson's coefficient of around 0.2 units (initial horizontal region) is evident from the behavior of all the mixtures. In the graph, the Poisson's ratio of the mixtures with II/B-S cement and fibers also show that their transversal strain remained in the same proportion to their longitudinal strain almost up until the maximum value (97–98%) of compressive strength. The circumstances of mixes IIIP-M and IISC differed, in so far as the Poisson's ratio reflected a notable increase of the transversal strain at stress levels of 60–70% of their compressive strength. The bridging effect caused by the presence of fibers against the tangential/circumferential tensile stresses, during the bulging of the specimens, yielded this singular behavior in mixes IISC-M and IISC-Y, unlike mixture IIIP-M, in all probability due to the different stiffness of the cementitious matrix.

4.3. Fiber pull-out test

A pull-out test was performed, in order to determine fiber adhesion within the concrete mass, following the instructions in ASTM C900-19 [51] and ACI 228.1R-03 [49]. The pull-out test measures the maximum force required to pull out an embedded fiber from within a concrete specimen. The pull-out force is applied by a loading system that raises an embedded fiber upwards from the surface of a concrete block secured in a clamp. Fig. 8 shows the arrangement of the test and its operation. In each fiber, the load versus the displacement (sum of the length of the extracted fiber and the elongation experienced by the fiber) was recorded. The test was performed on 13 fibers per mixture and both the average results, and the standard deviation (in brackets) are shown in Table 6. After the application of the load, all the fibers (metallic, polymeric) broke hardly without having moved, which leads us to conclude that the adhesion of both the metallic and the synthetic fibers within

Table 9
Characteristic values of stress-strain curves.

Mixture	Proportional limit			Maximum point			Failure strain		Absorbed energy (MJ/m^3)
	Stress (MPa)	Longitudinal strain (με)	Transverse strain (με)	Stress[1] (MPa)	Longitudinal strain (με)	Transverse strain (με)	Longitudinal strain (με)	Transverse strain (με)	
IISC	45.4	1131	256	77.8	2654	5854	2828	7455	0.1395
IISC-M	38.8	1117	250	63.3	3072	1722	3381	8058	0.1454
IISC-Y	34.6	1090	244	59.4	2926	1924	3220	7714	0.1302
IIIP-M	22.9	876	174	40.9	3619	5009	4269	8706	0.1351

[1] Different values from those in Table 6. Different specimens were used to obtain the compressive strength and stress-strain curves.

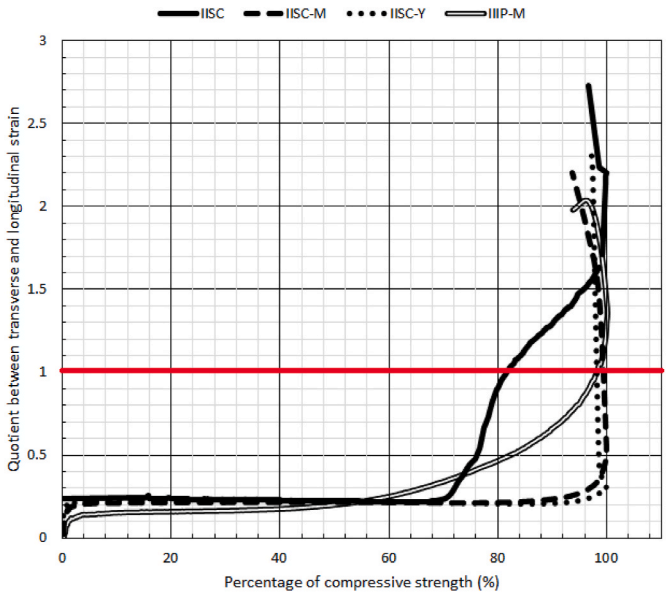

Fig. 7. Relationship between transversal and longitudinal strength.

the concrete mass was very good and was even better for the metallic fibers due to their ribbed ends. This adhesion, related to the ultimate pull out load, was mainly influenced by the type of fiber and its geometric and superficial characteristics, depth of embedment and the toughness of the cementitious matrix [70].

4.4. Indirect tensile strengths

Determining the tensile strength of concrete is no easy task with direct methods. For this reason, the determination of splitting tensile strength with the "Brazilian test" and the flexural strength test are widely used, due to their simplicity.

The splitting tensile strength test results, indirectly estimated from the Brazilian test on cylindrical 150 × 300-mm specimens after 90 days of curing, are shown in Table 6, 3.36 MPa for the IIIP-M mix and within a range of 4–5.1 MPa for the self-compacting mixtures manufactured with CEM II/B-S, respectively. Despite the presence of fibers in mixtures IISC-M (4.84 MPa) and IISC-Y (4.35 MPa), their splitting tensile strength values were lower than that of the reference mixture IISC without fibers (5.11 MPa). In all cases, the values were good, showing the excellent quality of the mixtures and their good tensile-resistant Interfacial Transition Zones (ITZ) between the EAFS and the cementitious paste [71,72].

The same trend was also observed for flexural strength at 90 days of curing obtained with 100 × 100 × 400-mm specimens in a three-point bending test. As shown in Table 6, the values of the self-compacting concretes were between 5 and 8 MPa, while the value of the pumpable concrete, IIIP-M, was 4.43 MPa. As with the previous test, the mixture without fibers, IISC, yielded the highest strength (7.93 MPa) followed by the IISC-M (5.97 MPa) and the IISC-Y (5.04 MPa) mixes.

Fibers sew the cracks that originate in concrete, which implies that the indirect tensile strengths of concrete increase [73]. This phenomenon is observed in SCC made with conventional aggregate [58] and in vibrated concrete made with large amounts of EAFS [36]. However, in this study, these strengths decreased with the addition of fibers, which was attributed to the notable increase of water required to ensure that the mixes retained flowability and that weakened the cementitious matrix. Therefore, the use of EAFS decreased the ability of the fibers to increase the tensile strength of SCC.

Both test results for mixture IIIP-M yielded the lowest values, despite the metallic fibers. Clearly, the cement type influenced the quality of the concrete and the bonds between the components (EAFS, cementitious matrix and fibers) of the ITZ.

4.4.1. Comparison with values from standards

The indirect tensile strength (f_t) of concrete can be estimated through either equation (6) (EC-2 and CEB-FIP [64,67]) or equation (7) (ACI-318 [63]). In turn, the flexural strength (f_{ft}) of concrete can be predicted by equations (8) and (9), which belong to EC-2 (CEB-FIP) and ACI-318 respectively. In these equations, R is the compressive strength of the concrete in MPa and h is the height of the tested specimen in mm.

$$\left.\begin{array}{l} f_t = 0.30\cdot(R-8)^{2/3} \text{ if } R \le 58\ MPa \\ f_t = 0.58\cdot(R-8)^{1/2} \text{ if } R>58\ MPa \end{array}\right\} \quad (6)$$

$$f_t = 0.56\cdot R^{0.5} \quad (7)$$

$$f_{ft} = max\left\{\left(1.6-\frac{h}{1,000}\right)\cdot f_t; f_t\right\} \quad (8)$$

$$f_{ft} = 0.94\cdot R^{0.5} \quad (9)$$

In Fig. 9, the comparison between the experimental and theoretical values of the formulas is shown. It can be seen that the adjustment was different for each indirect tensile strength. On the one hand, the splitting tensile strength was underestimated by both standards, with the ACI-318 [63] formulation showing the best fit, as for the modulus of elasticity. On the other, the flexural strength exhibited an intermediate adjustment, so that the results of the European formula applied to the mixtures with fibers fitted the experimental results better than the ACI formula [64,67], which in turn showed the best fit for the IISC mixture, without fibers [63]. Therefore, unlike the splitting tensile strength, no clear trend can be established regarding the best formulation for estimating the flexural strength of the mixtures.

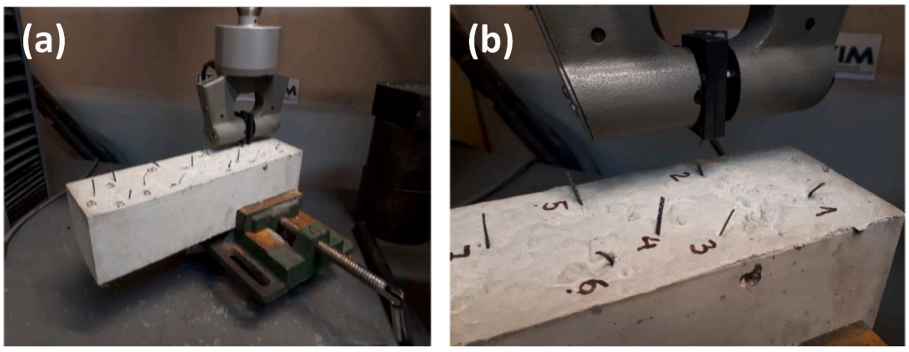

Fig. 8. Arrangement of the pull-out test: (a) Synthetic fiber pull out; (b) Synthetic fiber breakage.

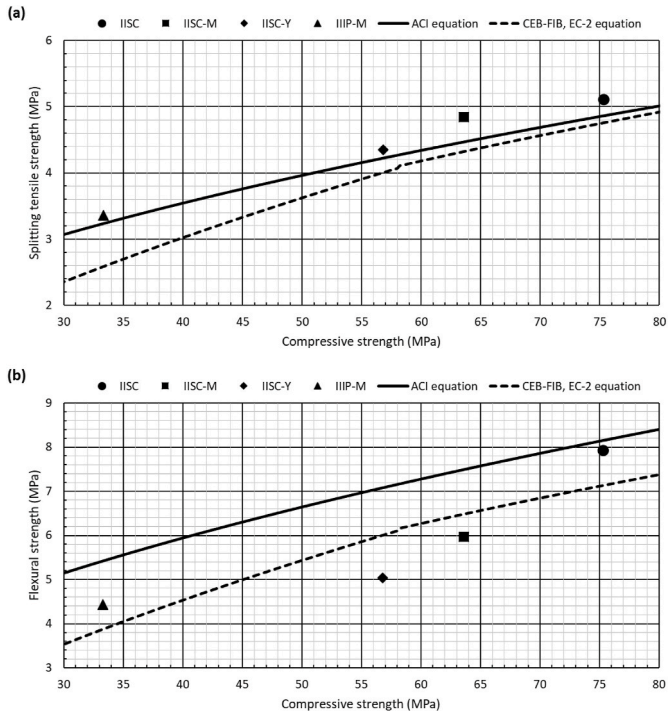

Fig. 9. Comparison of experimental indirect tensile strengths and theoretical values: (a) splitting tensile strength; (b) flexural strength.

4.5. Direct tensile strength: "dog-bone" test

Direct tensile tests are not widely used for concrete and there is a lack of guidance on how to perform this kind of test [51]. In this research, small sized dog-bone shaped specimens were used for the direct tension test, using two lateral Wheatstone-bridge gages to measure the longitudinal strain, as described in Fig. 10. The specimens underwent uniaxial tensile loading, and their tensile properties (direct tensile strength and tensile Young's modulus) are shown in Table 6. Furthermore, the stress-strain curves were likewise obtained, see Fig. 11.

In this research, a dog-bone mold was designed based on a review of Wille et al. [51] and the characteristics of the clamping jaws available in the laboratory. The test specimens were 164.1 mm in length with a 30 × 30-mm cross section, cured for 160 days in a moist room. Fig. 10 illustrates the specimen design, some tested specimens and the arrangement of the test.

The specimens were preloaded in six cycles of loading/unloading, see Fig. 11, to ensure proper alignment of the arrangement and to calculate the elastic modulus. The loading rate was 0.05 kN/s up to loads of 0.5, 0.75, 1, 1.5, 2, and 3 kN, respectively. Afterwards, they were loaded up to complete failure. The failure mode of the mixtures without fibers showed a brittle behavior when loaded beyond their ultimate tensile strength. Mixtures with fibers, especially the ones with steel fibers, showed a more ductile behavior; firstly, the concrete collapsed and then, the fibers. In the failure section, very few fibers were found parallel to the loading direction. The fibers that were properly oriented showed the same failure mode as the one observed in the pull-out test described above, *i.e.*, fiber breakage occurred.

The direct tensile test method showed lower tensile strengths than the Brazilian test, as suggested in other previous studies [74]. The values of direct tensile strength were 17%, 22%, 16% and 7% lower than the splitting tensile strength for mixtures IISC, IISC-M, IISC-Y and IIIP-M, respectively. Furthermore, the direct tensile strength was found at around 60–70% of the tensile stress from the flexural tests (Table 6).

Fig. 11 shows the stress-strain curve of each concrete in this direct tensile test, with a linear elastic behavior for mixtures IISC-M and IISC-M/Y. Slightly less linearity was observed in mixture IISC and a non-linear elastic behavior was observed for mixture IIIP-M which provided a curve with hysteresis. Both behaviors (non-linearity, hysteresis) noted in IIIP-M were thought to be related to the specific gels that form during the setting of CEM III/B concrete, based on the hydration of GGBFS. The use of EAFS resulted in failure strains similar to those obtained when using natural aggregate, regardless of fiber content and type [69]. Only the use of large amounts of GGBFS (IIIP-M mix) resulted in higher deformability of SCC under tensile stresses.

Although the results are quite rational, further research is needed, due to the "size effect" evident in the results of this direct tensile test [75]. The cross-section of the dog-bone should be carefully designed in accordance with both fiber and aggregate size. Otherwise, the fiber distribution might not be uniform, leaving areas without fibers at greater risk of brittle fracture.

The tensile Young's modulus tended to be slightly higher than the compressive Young's modulus for the mixtures with fibers (IISC-M/Y and IIIP), as also found in previous studies [74,76]. In the IISC mix, which did not incorporate fibers, a higher elastic stiffness in compres-

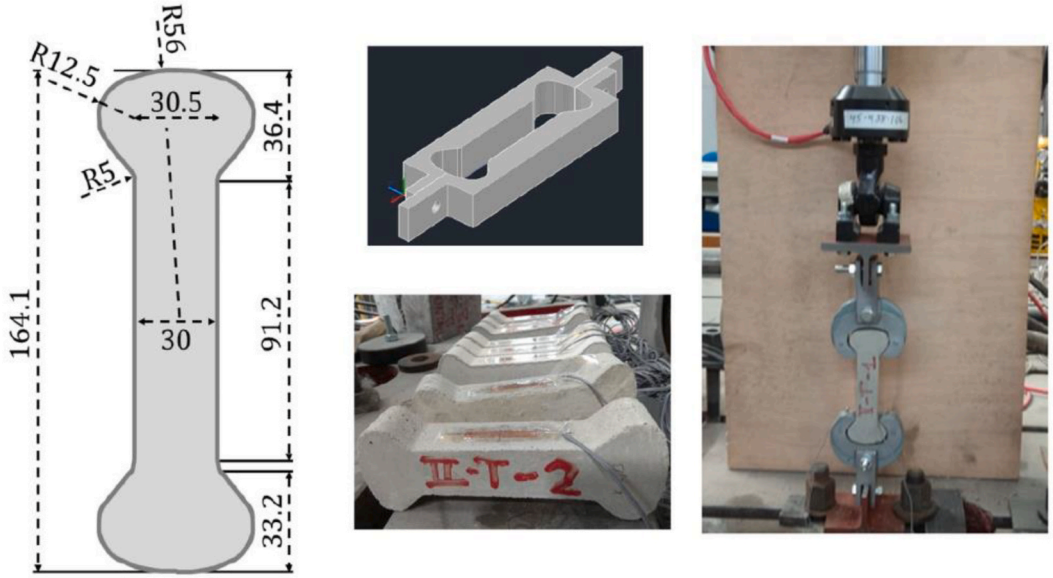

Fig. 10. Dog-bone design and arrangement of the direct tensile strength test.

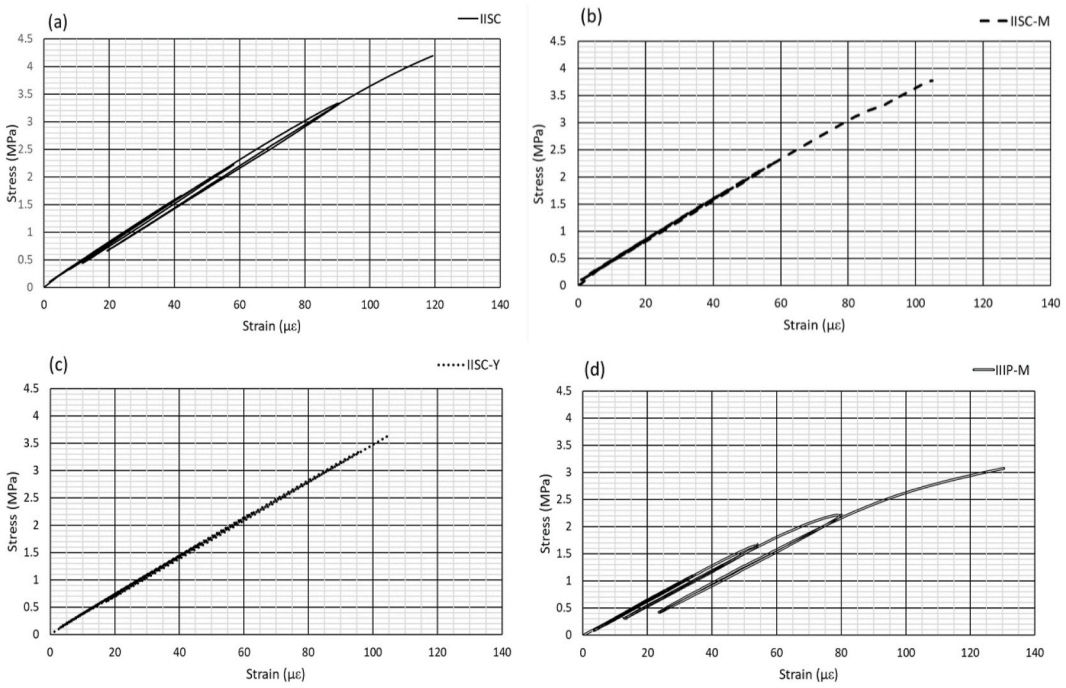

Fig. 11. Stress-strain curve of uniaxial tensile test: (a) IISC; (b) IISC-M; (c) IISC-Y; (d) IIIP-M.

sion was observed, as well as when using natural aggregate [69]. This trend is observed in Fig. 12, which shows the compressive moduli of mixes after 90 days of curing, depicted in Table 6, in comparison with the tensile moduli of mixes after 160 days of curing that are shown in Fig. 11. Generally, mixtures with metallic and polymeric fibers showed tensile elastic moduli values higher than their corresponding compressive moduli. The necessary correction, due to the different curing periods of the specimens, could be deduced from the data of Figs. 4 and 5, and should reduce the aforementioned difference. However, it is considered of less significance than the influence of the fibers within the concrete mass.

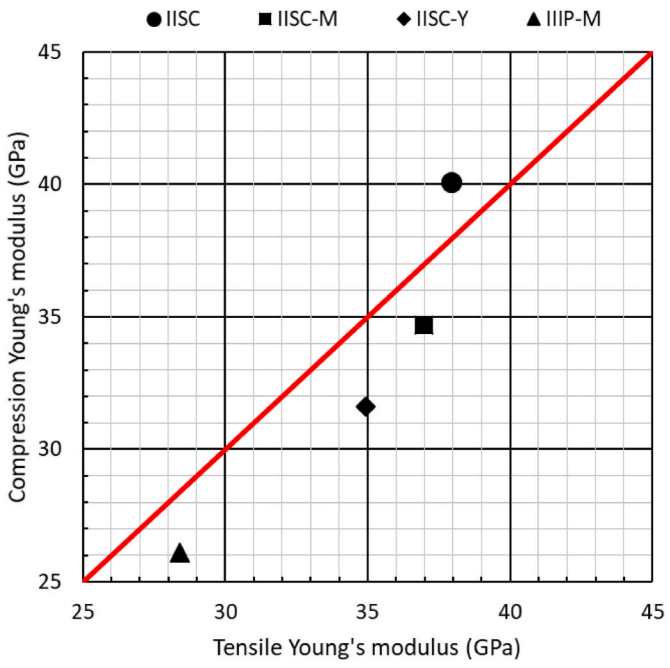

Fig. 12. Relationship between tensile and compressive elastic moduli.

4.6. Fracture toughness evaluation (with and without notching)

The fracture toughness of the mixtures is one of the most important characteristics that fibers provide to the concrete, enhancing its ductility in the post-cracking behavior [73]. Two bending tests were performed on specimens after 160 days curing in a moist room, to evaluate this property: the first one was a four-point test on 100 × 100 × 400-mm prismatic specimens with no notching, and the second one was a three-point test on 150 × 150 × 600-mm prismatic specimens with a 5-mm wide and 25-mm high notch [36], according to EN 83510 and EN 14651 + A1 [5], respectively. Three specimens of each mixture were used in each bending test. The implementation of these tests can be seen in Fig. 13 and Fig. 14. In both tests, a homogeneous behavior of the different specimens tested was observed, with no major differences between them, which allowed obtaining the average curves shown throughout this section. The results (average value and standard deviation) of both tests, shown in Table 10, refer to the following values: flexural toughness, initial cracking strength, LOP, residual strengths (F_{RJ}) and fracture energy (G_{F2} *and* $G_{F,CMOD}$).

Fig. 15 shows the load-deflection curves of the mixtures in the four-point bending test (with no notch), with a 300 mm span specimen. The deflection limit was established at 2 mm (according to the standard span of 300 mm divided by 150) and the area under the curves from the origin to the abscissa, 2 mm, was the flexural toughness value. The fracture energy was calculated by dividing the flexural toughness by the broken surface.

In the second bending test on a span of 550 mm, the Crack Mouth Opening Displacement (CMOD) was measured by an extensometer (Fig. 14b and c) and recorded while the notched specimens were loaded. The test was considered over when a CMOD of 4 mm was exceeded. Fig. 16 shows the curves of the load versus the CMOD where the origin and the abscissa, 3.5 mm, represents the validity limit of the test and, subsequently, the limit for the evaluation of the area under the curve.

In Figs. 15 and 16, a quite different post-peak behavior can be clearly observed in the mixtures. In the case of the reference mix (IISC), once it was cracked, the stresses were concentrated at crack tips, causing fast propagation up until fracture (brittle failure). Nevertheless, specimens with fibers were cracked, but not totally fractured, maintain-

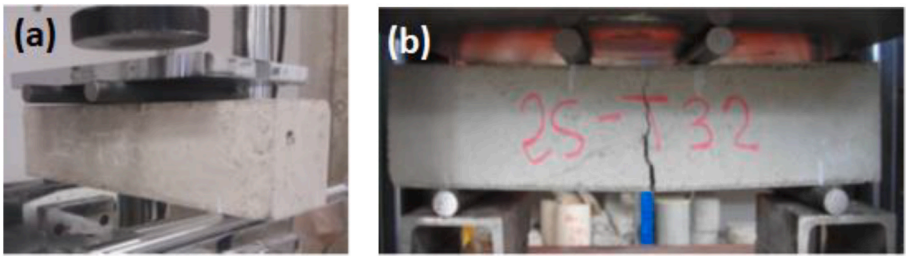

Fig. 13. First bending test performance: (a) test set up; (b) failure point.

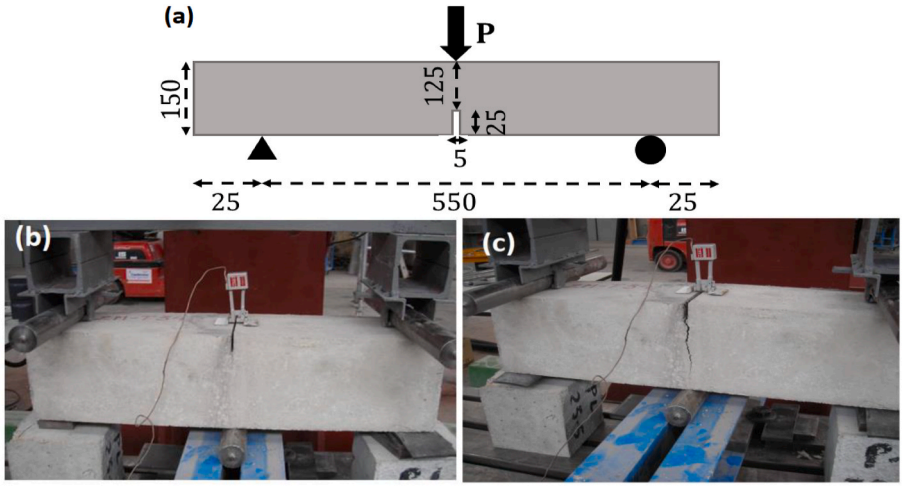

Fig. 14. Second bending test performance: (a) notch dimensions; (b) test set up; (c) failure point.

Table 10
Toughness and post-cracking behavior of the mixtures. Standard deviation in brackets.

Test	Property	Standard [5]	IISC	IISC-M	IISC-Y	IIIP-M
First bending test: four-point test on 100 × 100 × 400 mm prismatic specimens with no notch	Flexural toughness (N·m)	EN 83510	8.61 (1.2)	21.38 (1.7)	11.72 (1.1)	15.15 (1.3)
	First crack strength (MPa)		7.59 (2.1)	4.89 (1.4)	4.13 (0.5)	4.23 (0.7)
	Fracture energy, G_{F2} (N/mm)		0.880	2.153	1.190	1.533
Second bending test: three-point test on 150 × 150 × 600 mm prismatic specimens with a notch	Limit of proportionality LOP (MPa)	EN 14651 (notched specimens)	5.20 (0.8)	5.98 (1.1)	3.66 (0.4)	3.94 (0.3)
	F_{RJ1} (CMOD = 0.5)		–	6.52 (0.5)	1.21 (0.1)	2.37 (0.2)
	F_{RJ2} (CMOD = 1.5)		–	5.70 (0.3)	1.17 (0.1)	2.54 (0.1)
	F_{RJ3} (CMOD = 2.5)		–	3.96 (0.1)	1.29 (0.1)	2.72 (0.1)
	F_{RJ4} (CMOD = 3.5)		–	3.01 (0.1)	1.31 (0.1)	2.74 (0.1)
	Fracture energy (CMOD), $G_{F,CMOD}$ (N/mm)		0.162	2.637	0.707	1.378
	Fracture energy (CMOD), $G_{F,CMOD}$ (N/mm), in natural aggregate self-compacting concrete [58,77]		0.171	2.514	0.763	–

ing their load carrying capacity after the peak. Fibers crossed the crack and transferred the load due to the bridging effect. This sewing effect reduces the crack growth rate and improves concrete strength and toughness [78]. In both bending tests, the fibers that failed before completion presented the same failure mode as they did in the pull-out and dog-bone tests. Therefore, fiber breakage occurred, with optimum adherence between the fibers and the cementitious matrix.

In spite of the remarkable influence of the fibers in the post-cracking behavior, it can be observed that the initial crack strength followed the same tendency as the indirect and direct tensile strength tests of the mixtures previously detailed in Table 6. In this case, Fig. 15, the mixture without fibers, IISC, obtained the highest "first crack strength" (7.59 MPa), followed by IISC-M (4.89 MPa), IISC-Y (4.13 MPa) and IIIP-M (4.23 MPa). A significant effect of the fibers on the tensile state is observed in mixture IISC-M, in which the linear elastic field showed a notably higher slope than the one observed in the IISC mixture. When fibers are of the polymeric type the IISC-Y slope was close to that of a plain mixture. The lower quality mixture IIIP-M had the smallest slope.

The flexural toughness improvement (Table 10) of the mixture with metallic fibers, IISC-M (21.38 N m), with respect to the mix IISC (8.61 N m) was around 150%, while the improvement with synthetic fibers, in mixture IISC-Y, was around 35% (11.72 N m). The difference in post-cracking toughness was mainly due to the energy needed to pull out the fibers. Furthermore, the volume of synthetic fibers should have

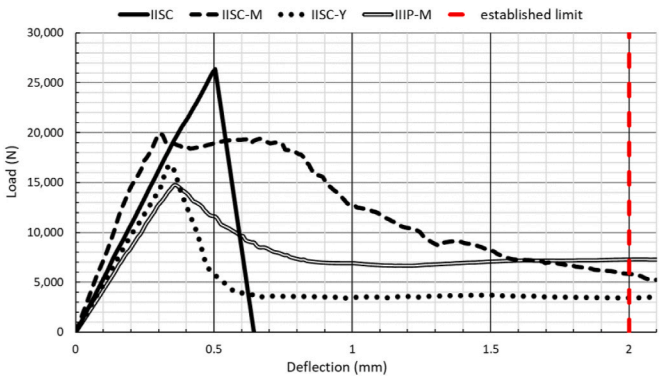

Fig. 15. Load versus deflection curves in four-point bending test of the mixtures.

been sufficient to maintain the horizontality of the curve and thus achieve acceptable results. The toughness result of IIIP-M (15.15 N m) was good despite its lower cement matrix quality.

According to the corresponding standard EN 14651, in the three-point bending test on the notched specimens (see Fig. 16), an important parameter is the Limit Of Proportionality (LOP), which is the stress of the initial elastic region that corresponds to the point of the load-CMOD curve where the shape loses perfect linearity, as detailed in Table 10. In this test, the LOP values were not aligned with the tendency observed for the flexural strength test curves, mainly due to the greater influence of the metallic fibers on the flexural stiffness of the mixtures. At this point, the stress in the presence of a notch increased in a different way. Mixture IISC-M yielded the best LOP result (5.98 MPa), followed by IISC (5.20 MPa) in which the decrease was notable; the sensitivity to notching was very pronounced in this case. Furthermore, mixture IISC-Y (3.66 MPa) showed the lowest LOP value, worse than that of mixture IIIP-M (3.94 MPa) containing metallic fibers. Subsequently, the initial cracking point corresponded to the maximum load recorded in the CMOD range between 0 and 0.05 mm. It approximately corresponds to the onset of cracking in the concrete matrix, as observed in Fig. 16b. In the same figure, the slightly higher slope of the IISC initial linear elastic region is also visible. Beyond this point, the fibers were more active in supporting the load. The effect of EAFS enhanced the beneficial effect of the metallic fibers, increasing the toughness of the SCC by 15% compared to the natural aggregate reference concrete with a cement content that was 50% higher [44,55].

From the residual flexural strengths of the fiber-reinforced mixtures, shown in Fig. 16, at CMODs of 0.5 (F_{RJ1}), 1.5 (F_{RJ2}), 2.5 (F_{RJ3}) and 3.5 mm (F_{RJ4}), it can be observed that the steel fibers, in mixture IISC-M (range of 3–6.5 MPa), increased these residual strengths between 3 and 6 times the strengths of the mixtures with synthetic fibers, IISC-Y (range of 1.2–1.3 MPa). On the other hand, mixture IIIP-M obtained good values of residual strengths, in the range of 2.4–2.7 MPa. The metallic fibers in the notched specimen tests evidently appeared to be much more decisive than in the unnotched specimen tests.

The fracture energies, G_{F2} and $G_{F,CMOD}$, represent the energy needed to create a unit area crack. The two values are defined as the area under the load-deflection curve (until an abscissa deflection of 2 mm) and the load-CMOD curve (until an abscissa CMOD of 3.5 mm), respectively, per unit surface area of fracture. In this study, the fracture energy was determined with the model proposed by Hillerborg [79]. The results in both tests were in general consistent, although a severe fall of fracture energy in the plain concrete (without fibers), mixture IISC, was evident when the specimens were notched. The toughness results clearly reflect the influence of the fibers on the fracture energy, the steel fibers providing better results than the polymeric ones. There were some slight differences between both fracture energy values in the fiber-reinforced concrete mixtures (with and without notching) (G_F *or* $G_{F,CMOD}$), as has also been reported in the literature [79].

4.7. Impact strength and abrasion resistance

The presence of fibers means that the concrete can absorb high impact energy thanks to the bridging effect of the fibers over the cracks. This effect means the concrete has high strength against brittle failure following impacts [36].

Cylindrical specimens of 150 mm in diameter and 63 ± 15 mm in height were prepared, in accordance with EN 83514 [25], by sawing ordinary specimens of 150 × 300 mm at a curing age of 160 days, in order to measure the impact strength of the concrete. These specimens were hit with a hammer weighing 4.534 ± 0.01 kg until an initial crack appeared and then repeatedly up until specimen breakage (Fig. 17). The results of this test are shown in Table 11, as the statistic mean value of eight sets of results, including data on the standard deviation. The values that were outside the mean range of impacts by ± 30% were rejected and a new mean value was calculated with the remaining values. The test may be considered valid when no more than two values differ by ± 30% from the mean.

In line with previous results, the mixture without fibers, IISC, in terms of number of hits until the initial cracking, had better results than those obtained by the mixtures IISC-Y and IIIP-M, despite their fiber content, which reminds us of the importance of the quality of the cementitious matrix. Otherwise, the metallic fibers in the IISC-M mixture notably improved its impact strength.

However, in terms of the number of hits until breakage, the results clearly showed the benefits of fiber-reinforced concretes. The strength until breakage of the mixtures with fibers was 4 times greater than the strength until the initial crack in mixture IISC-M, and was even 9 times greater in mixtures IISC-Y and IIIP-M. On the contrary, the mixture without fibers was at all times weaker. The fiber-reinforced mixtures, IISC-M, IISC-Y and IIIP-M exceeded the value of mixture IISC by 6, 5 and 2.5 times, respectively. A result that confirmed the outstanding improvement when fibers are added to slag-aggregate concrete, as reflected in the literature [71,80]. On the other hand, the addition of

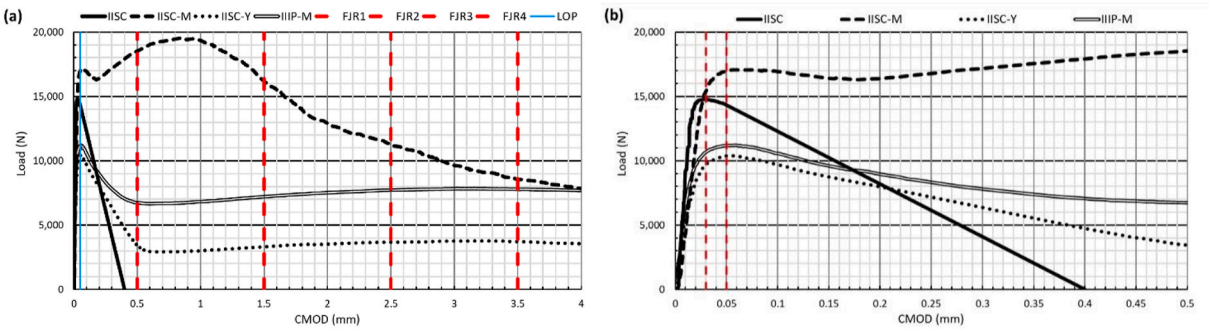

Fig. 16. Load versus CMOD curves in three-point bending test for notched specimens of the mixtures: (a) complete test; (b) up to a CMOD of 0.5 mm.

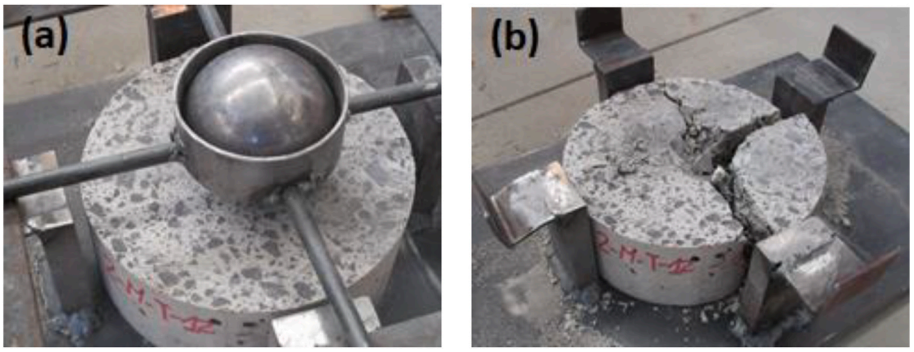

Fig. 17. Impact strength test: (a) test arrangement; (b) broken specimen.

Table 11
Impact strength and abrasion resistance test: average values and standard deviation between brackets.

		IISC	IISC-M	IISC-Y	IIIP-M
Impact strength	**Number of hits until first crack**	12.5 (1.7)	26.5 (3.5)	8.5 (1.7)	5.5 (0.6)
	Number of hits until breakage	16.0 (1.2)	99.3 (6.6)	78.3 (8.0)	40.2 (9.6)
Impact strength in conventional concrete [35,36]	**Number of hits until first crack**	6 (2.2)	19 (4.6)	16 (3.1)	–
	Number of hits until breakage	8 (2.7)	50 (6.1)	46 (5.3)	–
Abrasion resistance	**Footprint length (mm)**	74.5 (4.8)	80 (1.8)	83 (0.4)	84 (2.3)
	Footprint width (mm)	17 (3.0)	19 (0.5)	20 (0.3)	20.5 (1.2)

metallic fibers to EAFS concrete led to a higher increase in the impact strength of the mix than in concrete made with natural aggregate [54]. This behavior could have been due to the higher density and hardness of the EAFS, which enhanced the beneficial effect of the fibers [36].

The abrasion-resistance test, adapted to concrete in accordance with standards EN 1340 and EN 14157 can be used to evaluate surface performance, measured on an "internal" surface of mixtures, *i.e.*, on surfaces obtained by sawing ordinary 150 × 300-mm cylindrical specimens. In this study, this test was carried out at 360 days of curing aging, in order to evaluate the long-term surface concrete behavior against the abrasion-friction phenomenon, a tribological magnitude. The high-hardness surface of EAFS, which shows a high abrasion coefficient in the order of 57 units, explains the low values of footprint dimensions that are generally obtained when this aggregate is used in massive amounts [18]. These results are always better than those obtained with concrete produced with natural aggregate, in which the abrasion coefficient is usually between 40 and 50 units [28,36]. Nevertheless, the type of binder also influences this behavior [36]. The length and width of the footprint obtained for the mixtures in this study can be seen in Table 11. As in the other tests, mixture IISC showed the best behavior with the smallest footprint. The lower quality of the cementitious matrix of mixtures with fibers meant that the concrete surface was more sensitive to abrasion. In addition, the use of GGBFS and LFS (mixture IIIP-M) resulted in a less hard cement paste that caused the dimensions of the footprint to be larger.

5. Conclusions

In this paper, the mechanical behavior of high-workability (mostly self-compacting) concrete mixtures has been exhaustively evaluated. The concrete was manufactured with notable amounts (the highest possible) of Electric Arc Furnace Slag (EAFS) and Ground Granulated Blast Furnace Slag (GGBFS), as sustainable aggregates and binders, and smaller amounts of fibers (metallic and synthetic) and Ladle Furnace Slag (LFS) as Supplementary Cementitious Material (SCM). The conclusions of this work can be summarized as follows:

- The EAFS increased the loss of flowability of self-compacting concrete when adding fibers, compared to the natural aggregate mixes.
- Concrete strength and stiffness decreased in the EAFS fiber-reinforced self-compacting concretes with respect to the reference mixture without fibers. It is explained by the increase in the water/binder ratio that was necessary in the fiber-reinforced mixtures to reach the desired high workability in the fresh state. Similar behavior was noted in the natural aggregate concrete, in which elastic stiffness will not always increase following the addition of fibers.
- The greater presence of GGBFS and even the presence of LFS in mixture IIIP-M resulted in a mix with a weaker cementitious matrix that affected most of its mechanical properties. Furthermore, it led to a more compliant mixture, which showed the highest longitudinal failure strain at around 4300 με.
- The presence of fibers suppressed the yielding step obtained in the transverse direction and delayed the appearance of bulging in the specimens. The addition of EAFS had no effect on the longitudinal strain of the concrete, but increased its deformability in the transversal direction compared to conventional high-workability concrete.
- The indirect tensile strengths of fiber-reinforced concrete manufactured with CEM II/B-S were lower than those of non-fiber-reinforced concrete, mainly due to the higher quality of the cementitious matrix of the reference mixture. The increased proportion of water in the fiber-reinforced EAFS concrete to maintain high workability reduced the effectiveness of the fibers at increasing tensile strength observed in natural aggregate concrete. The pumpable concrete manufactured with CEM III/B showed lower indirect strengths than those obtained in mixtures with CEM II/B-S.
- The direct tensile dog-bone test results yielded lower tensile strength values than in the Brazilian test and the flexural tests for all the mixtures. The dog-bone test results will need further research, such as scaling the length and cross-section of fibers, to obtain optimum parameters related to tensile behavior and fracture energy of concrete mixtures.
- The pull-out test revealed good adhesion between the fibers, the aggregates, and the cementitious matrix within the concrete specimens.
- Steel fibers in amounts of 0.5% by volume of concrete remarkably improved the toughness and the ductile properties of the concrete. The use of EAFS also improved the post-cracking behavior. Nevertheless, the same volumes of synthetic fibers had no such beneficial effects on these properties.

- Impact strength was significantly increased with the addition of fibers, especially in concretes with steel fibers, as well as with the use of EAFS. On the contrary, the presence of fibers was not proven to be a determining factor in the abrasion resistance of the concretes under study.

Through all the tests presented in this article, it has been demonstrated that the structural use of high-workability fiber-reinforced concrete with massive amounts of slag as aggregate and binder is feasible from the point of view of their mechanical behavior. Furthermore, the deformational analysis (compression, tensile and bending) addressed in this study will, it is hoped, encourage other researchers to evaluate these aspects in sustainable concrete, given the very few studies on this subject in the literature.

CRediT authorship contribution statement

Vanesa Ortega-López: Conceptualization, Writing – original draft, Writing – review & editing, Project administration, Funding acquisition. **Aratz García-Llona:** Methodology, Data curation, Investigation, experimentation, Formal analysis. **Víctor Revilla-Cuesta:** Formal analysis, Data curation, experimentation, Writing – original draft, Writing – review & editing. **Amaia Santamaría:** Conceptualization, Methodology, experimentation, Investigation, Writing – review & editing. **José T. San-José:** Conceptualization, Methodology, Supervision, Writing – review & editing, Project administration, Funding acquisition.

Declaration of competing interest

The authors declare that they have no known competing financial interests or personal relationships that could have appeared to influence the work reported in this paper.

Acknowledgements

The authors wish to express their gratitude to the following entities for having funded this research work: the Spanish Ministries MCI, AEI, EU and ERDF [RTI2018-097079-B-C31; 10.13039/501100011033; FPU17/03374]; the Junta de Castilla y León (Regional Government) and ERDF [UIC-231, BU119P17]; the Basque Government research group [IT1314-19]; Youth Employment Initiative (JCyL) and ESF [UBU05B_1274]; the University of Burgos [Y135.GI] and the University of the Basque Country [PPGA20/26]. Likewise, our thanks to CHRYSO and HORMOR for supplying the materials used in this research.

References

[1] M.B. Ali, R. Saidur, M.S. Hossain, A review on emission analysis in cement industries, Renew. Sustain. Energy Rev. 15 (5) (2011) 2252–2261, https://doi.org/10.1016/j.rser.2011.02.014.
[2] F. Orsini, P. Marrone, Approaches for a low-carbon production of building materials: a review, J. Clean. Prod. 241 (2019) 118380, https://doi.org/10.1016/j.jclepro.2019.118380.
[3] V. Revilla-Cuesta, M. Skaf, F. Faleschini, J.M. Manso, V. Ortega-López, Self-compacting concrete manufactured with recycled concrete aggregate: an overview, J. Clean. Prod. 262 (2020) 121362, https://doi.org/10.1016/j.jclepro.2020.121362.
[4] L. Barcelo, J. Kline, G. Walenta, E. Gartner, Cement and carbon emissions, Mater. Struct. 47 (6) (2014) 1055–1065, https://doi.org/10.1617/s11527-013-0114-5.
[5] EN-Euronorm, Rue de stassart, 36. Belgium-1050 Brussels, European Committee for Standardization.
[6] S.I. Abu-Eishah, A.S. El-Dieb, M.S. Bedir, Performance of concrete mixtures made with electric arc furnace (EAF) steel slag aggregate produced in the Arabian Gulf region, Construct. Build. Mater. 34 (2012) 249–256, https://doi.org/10.1016/j.conbuildmat.2012.02.012.
[7] B. Xu, Y. Yi, Soft clay stabilization using ladle slag-ground granulated blastfurnace slag blend, Appl. Clay Sci. 178 (2019) 105136, https://doi.org/10.1016/j.clay.2019.105136.
[8] M.I. Prieto, M.N. González, Á. Rodríguez, A. Cobo, The influence of replacing aggregates and cement by LFS on the corrosion of steel reinforcements, Appl. Sci. 9 (4) (2019) 683, https://doi.org/10.3390/app9040683.
[9] K.K. Sideris, C. Tassos, A. Chatzopoulos, P. Manita, Mechanical characteristics and durability of self compacting concretes produced with ladle furnace slag, Construct. Build. Mater. 170 (2018) 660–667, https://doi.org/10.1016/j.conbuildmat.2018.03.091.
[10] F. Faleschini, A. Santamaria, M.A. Zanini, J.T. San José, C. Pellegrino, Bond between steel reinforcement bars and electric arc furnace slag concrete, Mater. Struct. 50 (3) (2017) 170, https://doi.org/10.1617/s11527-017-1038-2.
[11] A. Santamaría, J.J. González, M.M. Losáñez, M. Skaf, V. Ortega-López, The design of self-compacting structural mortar containing steelmaking slags as aggregate, Cement Concr. Compos. 111 (2020) 103627, https://doi.org/10.1016/j.cemconcomp.2020.103627.
[12] F. Maghool, A. Arulrajah, C. Suksiripattanapong, S. Horpibulsuk, A. Mohajerani, Geotechnical properties of steel slag aggregates: shear strength and stiffness, Soils Found. (2019), https://doi.org/10.1016/j.sandf.2019.03.016.
[13] V. Ortega-López, M. Skaf, A. Santamaría, The reuse of ladle furnace basic slags in clayey soil-stabilization applications, Soil Stabilization: types, Methods and Applications, Nova Science Publishers, Inc (2017) 231–271.
[14] M. Pasetto, A. Baliello, E. Pasquini, M. Skaf, V. Ortega-López, Performance-based characterization of bituminous mortars prepared with ladle furnace steel slag, Sustainability 12 (5) (2020) 1777, https://doi.org/10.3390/su12051777.
[15] J.M. Terrones-Saeta, F.J. Iglesias-Godino, F.A. Corpas-Iglesias, C. Martínez-García, Study of the incorporation of ladle furnace slag in the manufacture of cold in-place recycling with bitumen emulsion, Materials 13 (21) (2020) 4765, https://doi.org/10.3390/ma13214765.
[16] B. Fronek, P. Bosela, N. Delatte, Steel slag aggregate used in Portland cement concrete, Transport. Res. Rec. 2267 (2012) 37–42, https://doi.org/10.3141/2267-04.
[17] L. Rondi, G. Bregoli, S. Sorlini, L. Cominoli, C. Collivignarelli, G. Plizzari, Concrete with EAF steel slag as aggregate: a comprehensive technical and environmental characterisation, Compos. B Eng. 90 (2016) 195–202, https://doi.org/10.1016/j.compositesb.2015.12.022.
[18] M. Skaf, J.M. Manso, Á. Aragón, J.A. Fuente-Alonso, V. Ortega-López, EAF slag in asphalt mixes: a brief review of its possible re-use, Resour. Conserv. Recycl. 120 (2017) 176–185, https://doi.org/10.1016/j.resconrec.2016.12.009.
[19] I. Rodríguez-Fernández, P. Lastra-González, I. Indacoechea-Vega, D. Castro-Fresno, Technical feasibility for the replacement of high rates of natural aggregates in asphalt mixtures, Int. J. Pavement Eng. (2019), https://doi.org/10.1080/10298436.2019.1654102.
[20] I.Z. Yildirim, M. Prezzi, Subgrade stabilisation mixtures with EAF steel slag: an experimental study followed by field implementation, Int. J. Pavement Eng. (2020), https://doi.org/10.1080/10298436.2020.1823389.
[21] M. Papachristoforou, I. Papayianni, Radiation shielding and mechanical properties of steel fiber reinforced concrete (SFRC) produced with EAF slag aggregates, Radiat. Phys. Chem. 149 (2018) 26–32, https://doi.org/10.1016/j.radphyschem.2018.03.010.
[22] B. Pomaro, F. Gramegna, R. Cherubini, V. De Nadal, V. Salomoni, F. Faleschini, Gamma-ray shielding properties of heavyweight concrete with Electric Arc Furnace slag as aggregate: an experimental and numerical study, Construct. Build. Mater. 200 (2019) 188–197, https://doi.org/10.1016/j.conbuildmat.2018.12.098.
[23] H.S. Lim, H.S. Lee, S.J. Kwon, Mechanical properties and radiation shielding performance in concrete with electric arc furnace oxidizing slag aggregate, J. Ceram. Process. Res. 20 (4) (2019) 363–371.
[24] M. Skaf, E. Pasquini, V. Revilla-Cuesta, V. Ortega-Lopez, Performance and durability of porous asphalt mixtures manufactured exclusively with electric steel slags, Materials 12 (20) (2019) 3306, https://doi.org/10.3390/ma12203306.
[25] R. Vaiana, F. Balzano, T. Iuele, V. Gallelli, Microtexture performance of EAF slags used as aggregate in asphalt mixes: a comparative study with surface properties of natural stones, Appl. Sci. 9 (15) (2019) 3197, https://doi.org/10.3390/app9153197.
[26] F. Gulisano, J. Crucho, J. Gallego, L. Picado-Santos, Microwave healing performance of asphalt mixture containing electric arc furnace (EAF) slag and graphene nanoplatelets (GNPs), Appl. Sci. 10 (4) (2020) 1428, https://doi.org/10.3390/app10041428.
[27] N. Hani, O. Nawawy, K.S. Ragab, M. Kohail, The effect of different water/binder ratio and nano-silica dosage on the fresh and hardened properties of self-compacting concrete, Construct. Build. Mater. 165 (2018) 504–513, https://doi.org/10.1016/j.conbuildmat.2018.01.045.
[28] S. Pranav, S. Aggarwal, E.H. Yang, A. Kumar Sarkar, A. Pratap Singh, M. Lahoti, Alternative materials for wearing course of concrete pavements: a critical review, Construct. Build. Mater. 236 (2020) 117609, https://doi.org/10.1016/j.conbuildmat.2019.117609.
[29] S. Tomasiello, M. Felitti, EAF slag in self-compacting concretes, Facta Univ. – Ser. Archit. Civ. Eng. 8 (1) (2010) 13–21, https://doi.org/10.2298/fuace1001013t.
[30] Y.N. Sheen, D.H. Le, T.H. Sun, Innovative usages of stainless steel slags in developing self-compacting concrete, Construct. Build. Mater. 101 (2015) 268–276, https://doi.org/10.1016/j.conbuildmat.2015.10.079.
[31] P. Zampieri, N. Simoncello, J. Gonzalez Libreros, C. Pellegrino, Bond behavior of steel fiber-reinforced mortar (SFRM) applied onto masonry substrate, Arch. Civ. Mech. Eng. 20 (3) (2020) 92, https://doi.org/10.1007/s43452-020-00090-6.
[32] D.Y. Yoo, M.C. Kang, H.J. Choi, W. Shin, S. Kim, Influence of chemically treated carbon fibers on the electromagnetic shielding of ultra-high-performance fiber-reinforced concrete, Arch. Civ. Mech. Eng. 20 (4) (2020) 123, https://doi.org/10.1007/s43452-020-00117-y.
[33] S. Yazici, G. Inan, V. Tabak, Effect of aspect ratio and volume fraction of steel fiber on the mechanical properties of SFRC, Construct. Build. Mater. 21 (6) (2007)

1250–1253, https://doi.org/10.1016/j.conbuildmat.2006.05.025.
[34] J.T. San-José, J.M. Manso, Fiber-reinforced polymer bars embedded in a resin concrete: study of both materials and their bond behavior, Polym. Compos. 27 (3) (2006) 315–322, https://doi.org/10.1002/pc.20188.
[35] P. Rossi, E. Parant, Damage mechanisms analysis of a multi-scale fibre reinforced cement-based composite subjected to impact and fatigue loading conditions, Cement Concr. Res. 38 (3) (2008) 413–421, https://doi.org/10.1016/j.cemconres.2007.09.002.
[36] J.A. Fuente-Alonso, V. Ortega-López, M. Skaf, Á. Aragón, J.T. San-José, Performance of fiber-reinforced EAF slag concrete for use in pavements, Construct. Build. Mater. 149 (2017) 629–638, https://doi.org/10.1016/j.conbuildmat.2017.05.174.
[37] B. Belletti, R. Cerioni, A. Meda, G. Plizzari, Design aspects on steel fiber-reinforced concrete pavements, J. Mater. Civ. Eng. 20 (9) (2008) 599–607 (2008)20:9(599), https://doi.org/10.1061/(ASCE)0899-1561.
[38] Y. Zhang, J. Fan, W. Fan, Seismic fragility analysis of concrete bridge piers reinforced by steel fibers, Adv. Struct. Eng. 19 (5) (2016) 837–848, https://doi.org/10.1177/1369433216630440.
[39] H.H. Lee, Shear strength and behavior of steel fiber reinforced concrete columns under seismic loading, Eng. Struct. 29 (7) (2007) 1253–1262, https://doi.org/10.1016/j.engstruct.2006.08.016.
[40] B. Chiaia, A.P. Fantilli, P. Vallini, Combining fiber-reinforced concrete with traditional reinforcement in tunnel linings, Eng. Struct. 31 (7) (2009) 1600–1606, https://doi.org/10.1016/j.engstruct.2009.02.037.
[41] B. Golestani, H. Maherinia, B.H. Nam, A. Behzadan, Investigation on the effects of recycled asphalt shingle as an additive to hot-mix asphalt, Proceedings of International Airfield and Highway Pavements Conference: Innovative and Cost-Effective Pavements for a Sustainable Future, American Society of Civil Engineers (ASCE), 2015, pp. 9–18.
[42] E.K. Anastasiou, I. Papayianni, M. Papachristoforou, Behavior of self compacting concrete containing ladle furnace slag and steel fiber reinforcement, Mater. Des. 59 (2014) 454–460, https://doi.org/10.1016/j.matdes.2014.03.030.
[43] B. Xu, Y. Yi, Use of ladle furnace slag containing heavy metals as a binding material in civil engineering, Sci. Total Environ. 705 (2020) 135854, https://doi.org/10.1016/j.scitotenv.2019.135854.
[44] A. Santamaría, V. Ortega-López, M. Skaf, J.A. Chica, J.M. Manso, The study of properties and behavior of self compacting concrete containing Electric Arc Furnace Slag (EAFS) as aggregate, Ain Shams Eng. J. 11 (1) (2020) 231–243, https://doi.org/10.1016/j.asej.2019.10.001.
[45] H. Qasrawi, Fresh properties of green SCC made with recycled steel slag coarse aggregate under normal and hot weather, J. Clean. Prod. 204 (2018) 980–991, https://doi.org/10.1016/j.jclepro.2018.09.075.
[46] V. Ortega-López, J.M. Manso, I.I. Cuesta, J.J. González, The long-term accelerated expansion of various ladle-furnace basic slags and their soil-stabilization applications, Construct. Build. Mater. 68 (2014) 455–464, https://doi.org/10.1016/j.conbuildmat.2014.07.023.
[47] J.M. Manso, D. Hernández, M.M. Losáñez, J.J. González, Design and elaboration of concrete mixtures using steelmaking slags, ACI Mater. J. 108 (6) (2011) 673–681.
[48] EFNARC, Specification Guidelines for Self-Compacting Concrete, European Federation of National Associations Representing producers and applicators of specialist building products for Concrete, 2002.
[49] UNE-EN 206, +A1 Standars. Hormigón: Especificaciones, Prestaciones, Producción Y Conformidad, AENOR, Madrid, Spain, 2003.
[50] UNE-83514, Concrete with Fibres, Determination of the impact strength, 2005.
[51] K. Wille, S. El-Tawil, A.E. Naaman, Properties of strain hardening ultra high performance fiber reinforced concrete (UHP-FRC) under direct tensile loading, Cement Concr. Compos. 48 (2014) 53–66, https://doi.org/10.1016/j.cemconcomp.2013.12.015.
[52] ASTM-C900-19, Standard Test Method for Pullout Strength of Hardened Concrete, 2019.
[53] ACI-228.1R-19, In-place Methods to Estimate Concrete Strength, 2019.
[54] N. Li, Z. Jin, G. Long, L. Chen, Q. Fu, Y. Yu, X. Zhang, C. Xiong, Impact resistance of steel fiber-reinforced self-compacting concrete (SCC) at high strain rates, J. Build. Eng. 38 (2021) 102212, https://doi.org/10.1016/j.jobe.2021.102212.
[55] A. Sadrmomtazi, S.H. Gashti, B. Tahmouresi, Residual strength and microstructure of fiber reinforced self-compacting concrete exposed to high temperatures, Construct. Build. Mater. 230 (2020) 116969, https://doi.org/10.1016/j.conbuildmat.2019.116969.
[56] V. Ortega-López, J.A. Fuente-Alonso, A. Santamaría, J.T. San-José, Á. Aragón, Durability studies on fiber-reinforced EAF slag concrete for pavements, Construct. Build. Mater. 163 (2018) 471–481, https://doi.org/10.1016/j.conbuildmat.2017.12.121.
[57] H. Yi, G. Xu, H. Cheng, J. Wang, Y. Wan, H. Chen, An Overview of Utilization of Steel Slag 16 (2012) 791–801, https://doi.org/10.1016/j.proenv.2012.10.108.
[58] M.G. Alberti, A. Enfedaque, J.C. Gálvez, A. Cortez, Optimisation of fibre reinforcement with a combination strategy and through the use of self-compacting concrete, Construct. Build. Mater. 235 (2020) 117289, https://doi.org/10.1016/j.conbuildmat.2019.117289.
[59] N. Carino, H. Lew, The maturity method: from theory to application, 2001, pp. 1–19 (2001)17, https://doi.org/10.1061/40558.
[60] T. Knudsen, The dispersion model for hydration of portland cement I. General concepts, Cement Concr. Res. 14 (5) (1984) 622–630, https://doi.org/10.1016/0008-8846(84)90024-3.
[61] P. Freiesleben Hansen, J. Pedersen, Curing of Concrete Structures, 1985, p. 166.
[62] F. Bencardino, L. Rizzuti, G. Spadea, R.N. Swamy, Stress-strain behavior of steel fiber-reinforced concrete in compression, J. Mater. Civ. Eng. 20 (3) (2008) 255–263 (2008)20:3(255), https://doi.org/10.1061/(ASCE)0899-1561.
[63] ACI-318-19, Building Code Requeriments for Structural Concrete, 2019.
[64] CEB-FIB, Model Code Volumes 1 and 2 Volumes 1 and 2 (2010) (2012).
[65] S. Anandan, S. Islam, R.A. Khan, Effect of steel fibre profile on the fracture characteristics of steel fibre reinforced concrete beams, J. Eng. Res. (Kuwait) 7 (2) (2019) 105–124.
[66] V.S. Bharath, P.R.M. Rao, Study on the fibre reinforced concrete using steel slag as the coarse aggregate replacement, Int. J. Technol. Res. Eng. 2 (7) (2015).
[67] EC-2, Eurocode 2: Design of Concrete Structures. Part 1-1: General Rules and Rules for Buildings, CEN (European Committee for Standardization), 2010.
[68] EHE-08, Instrucción de Hormigón Estructural, Structural Concrete Regulations, Ministerio de Fomento, Gobierno de España, 2010.
[69] A. Karimipour, M. Edalati, J. de Brito, Biaxial mechanical behaviour of polypropylene fibres reinforced self-compacting concrete, Construct. Build. Mater. 278 (2021) 122416, https://doi.org/10.1016/j.conbuildmat.2021.122416.
[70] R. Ballarini, S.P. Shah, L.M. Keer, Failure characteristics of short anchor bolts embedded in a brittle material, Proc. R. Soc. London Ser. A 404 (1826) (1986) 35–54.
[71] S. Amelian, M. Manian, S.M. Abtahi, A. Goli, Moisture sensitivity and mechanical performance assessment of warm mix asphalt containing by-product steel slag, J. Clean. Prod. 176 (2018) 329–337, https://doi.org/10.1016/j.jclepro.2017.12.120.
[72] A.S. Brand, J.R. Roesler, Interfacial transition zone of cement composites with steel furnace slag aggregates, Cement Concr. Compos. 86 (2018) 117–129, https://doi.org/10.1016/j.cemconcomp.2017.11.012.
[73] N. Banthia, M. Sappakittipakorn, Toughness enhancement in steel fiber reinforced concrete through fiber hybridization, Cement Concr. Res. 37 (9) (2007) 1366–1372, https://doi.org/10.1016/j.cemconres.2007.05.005.
[74] D. Shen, X. Shi, S. Zhu, X. Duan, J. Zhang, Relationship between tensile Young's modulus and strength of fly ash high strength concrete at early age, Construct. Build. Mater. 123 (2016) 317–326, https://doi.org/10.1016/j.conbuildmat.2016.06.145.
[75] J.G.M. Van Mier, M.R.A. Van Vliet, Influence of microstructure of concrete on size/scale effects in tensile fracture, Eng. Fract. Mech. 70 (16) (2003) 2281–2306, https://doi.org/10.1016/S0013-7944(02)00222-9.
[76] I. Yoshitake, W. Zhang, Y. Mimura, T. Saito, Uniaxial tensile strength and tensile Young's modulus of fly-ash concrete at early age, Construct. Build. Mater. 40 (2013) 514–521, https://doi.org/10.1016/j.conbuildmat.2012.11.022.
[77] F. Soltanzadeh, V.M.C.F. Cunha, J.A.O. Barros, Assessment of different methods for characterization and simulation of post-cracking behavior of self-compacting steel fiber reinforced concrete, Construct. Build. Mater. 227 (2019) 116704, https://doi.org/10.1016/j.conbuildmat.2019.116704.
[78] H.R. Pakravan, M. Latifi, M. Jamshidi, Hybrid short fiber reinforcement system in concrete: a review, Construct. Build. Mater. 142 (2017) 280–294, https://doi.org/10.1016/j.conbuildmat.2017.03.059.
[79] A. Hillerborg, Results of three comparative test series for determining the fracture energy GF of concrete, Mater. Struct. 18 (5) (1985) 407–413, https://doi.org/10.1007/BF02472416.
[80] C. Pellegrino, V. Gaddo, Mechanical and durability characteristics of concrete containing EAF slag as aggregate, Cement Concr. Compos. 31 (9) (2009) 663–671, https://doi.org/10.1016/j.cemconcomp.2009.05.006.